

Functionalized Carbon Spheres for Energy-Efficient CO₂ Capture: Synthesis, Application, and Reaction Mechanism

Umair H. Bhatti, Masood S. Alivand, Francesco Barzaghi, Meher Geetika Sanku, Jorge Gascon,* and Kathryn A. Mumford*



Cite This: *ACS Sustainable Chem. Eng.* 2023, 11, 11955–11964



Read Online

ACCESS |

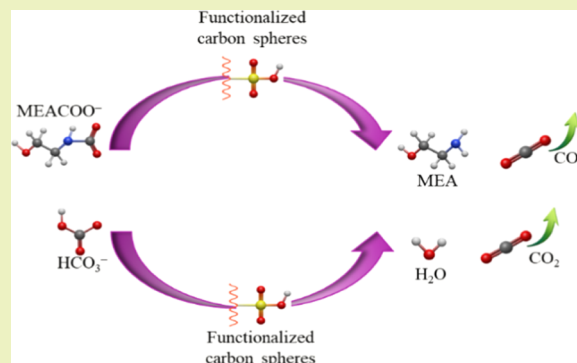
Metrics & More

Article Recommendations

Supporting Information

ABSTRACT: Catalyst-facilitated amine regeneration provides exciting new opportunities to fulfill the Paris Climate Accord by developing an energy-efficient and economically feasible CO₂ capture process. However, finding inexpensive and easy-to-synthesize catalysts, along with understanding the catalytic desorption mechanism, is imperative. Herein, we develop an environmentally friendly glucose-derived carbon sphere nanocatalyst with isethionic acid functionalization which can optimize the CO₂ desorption rate of CO₂-loaded aqueous monoethanolamine (MEA) solutions at ~86 °C. The desired physicochemical properties of the developed materials can be readily tuned by varying the amount of isethionic acid used for functionalization. The synthesized catalysts accelerated the CO₂ desorption rate by up to 108% and reduced the heat duty by ~10.8% compared to the traditional uncatalyzed MEA regeneration. NMR analysis unveils that unlike conventional regeneration where carbamate stability hinders the low-temperature CO₂ desorption, the prepared catalysts can decompose carbamate at much lower temperatures and thereby reduce the energy consumption of amine regeneration. These catalysts can be readily separated and are stable in cyclic uses, making them suitable for industrial-scale applications. Catalyst-facilitated solvent regeneration at 86 °C can allow the regenerator to use low-grade industrial waste heat, which may enable efficient CO₂ capture facilities to be installed at a wide range of industrial sites to achieve net zero emissions by 2050.

KEYWORDS: catalytic regeneration, glucose-derived nanocatalyst, energy-efficient CO₂ capture, CO₂ desorption, heat duty



INTRODUCTION

Despite significant growth in renewable energy sources, fossil fuels still account for nearly 80% of global energy, resulting in the emission of 36.3 gigatons of CO₂ in 2021.¹ Given that fossil fuels are projected to remain the dominant energy source in the coming decades, an effective short- to mid-term solution is to install CO₂ capture facilities at large CO₂ emission sources, e.g., coal-fired power plants, which account for nearly 40% of global CO₂ emissions.^{2,3} Chemical absorption of CO₂ from flue gas streams using aqueous alkanolamines is a technically mature and commercially available technique for this purpose.^{4,5} In this process, CO₂ is selectively absorbed into the amines via exothermic reactions, forming carbamate and bicarbonate. In the second step, the absorption reactions are reversed at higher temperatures to break the carbamate, eventually separating the amine and CO₂, thereby regenerating the solvent for reuse. The main drawback of this process is the large energy required to heat the solvent during solvent regeneration, which accounts for nearly 70% of the total process operating cost.^{6,7} Poor CO₂ desorption kinetics necessitate the regeneration process to be carried out at temperatures greater than 120 °C. As reactive amine solutions

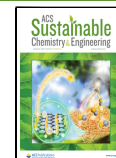
are primarily water-based, massive quantities of thermal energy are required to heat and boil the water.

Recent research efforts have focused on developing advanced absorbents that require lower amounts of energy for solvent regeneration. For instance, instead of using a single amine, multiple amines of complementing nature can be blended to achieve a greater CO₂ absorption capacity and low energy consumption for solvent regeneration.^{8–10} Biphasic solvents also offer the potential for low energy consumption due to their ability to form two phases after CO₂ absorption, whereby the CO₂-rich phase can be separated and regenerated, hence saving the energy associated with heating the CO₂-lean phase.^{11–13} Deep eutectic solvents can be suitable candidates for their interesting properties such as low volatility, high thermal stability, and less energy-intensive regeneration.^{14,15}

Received: April 6, 2023

Revised: July 4, 2023

Published: August 1, 2023



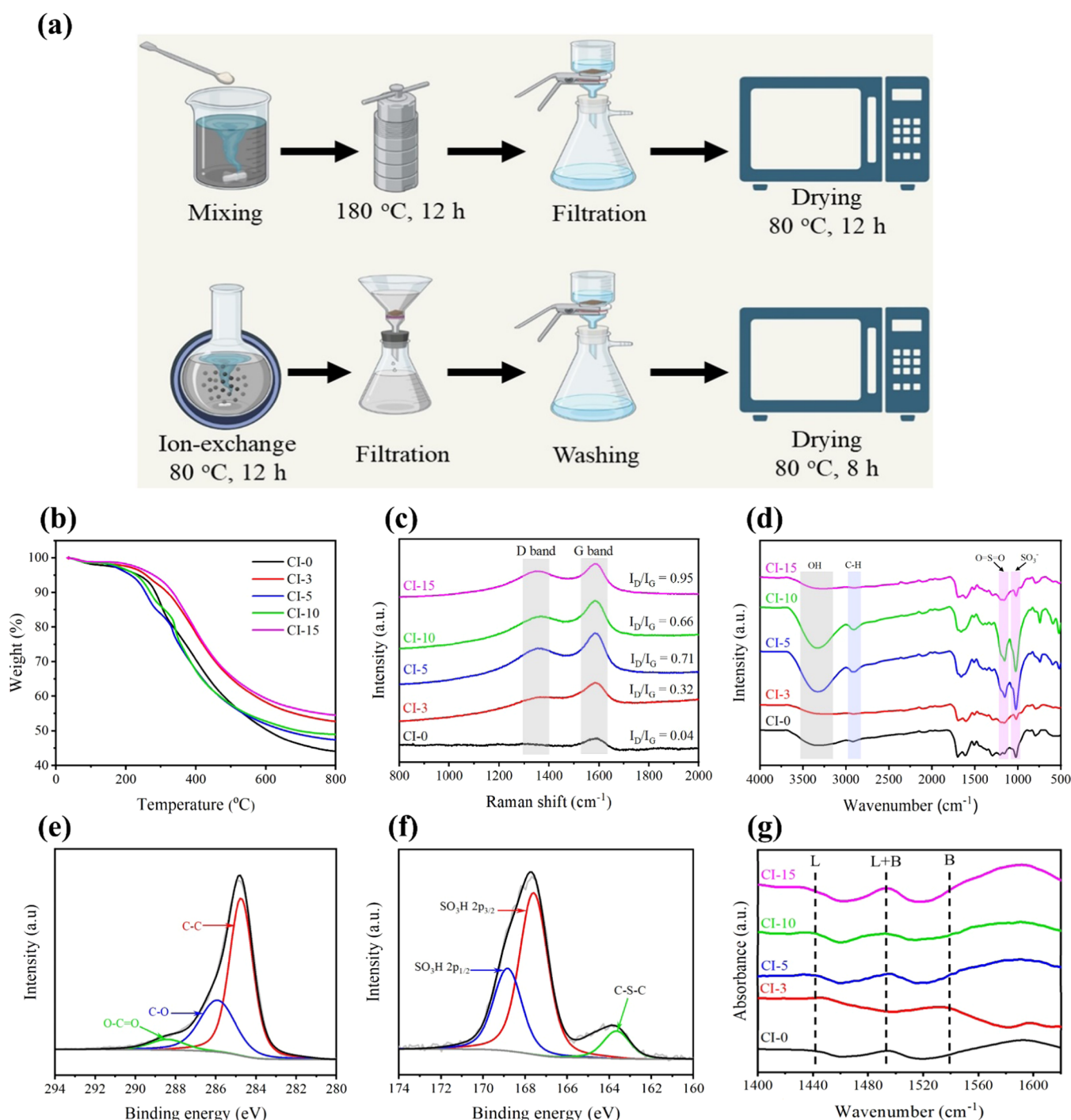


Figure 1. (a) Main steps involved in the preparation of isethionic acid-functionalized carbon spheres. Characterization results of carbon spheres before and after sulfonation. (b) TGA curves, (c) Raman spectra, (d) FT-IR spectra, and (e) C 1s XPS spectra of CI-0, (f) S 2p XPS spectra of CI-15, and (g) pyridine FT-IR spectra.

Since the use of water as a cosolvent is a key driver for the high heat duty of conventional aqueous absorbents, water-lean and nonaqueous absorbents have been designed by replacing water with organic diluents that have a lower heat capacity and vaporization heat compared to water.^{16–19} Although these new solvents are claimed to reduce the regeneration energy penalty to 2.1–2.4 GJ/tCO₂, their technical and operational feasibility is yet to be proven.²⁰

Another interesting strategy to reduce the absorbent regeneration penalty is to add a solid acidic catalyst to

optimize CO₂ desorption at lower temperatures. The incorporation of a solid catalyst introduces acid sites (Lewis and Brønsted acid sites) that can facilitate carbamate breakdown and promote proton transfer between different species to enable CO₂ release at low temperatures.^{21–23} With a higher CO₂ desorption rate at relatively lower temperatures, solvent regeneration can then be performed at <100 °C, which not only reduces the regeneration heat duty but also allows the use of waste heat to run the regeneration process. Idem et al. first reported in 2011 that HZSM-5 and γ-Al₂O₃ catalysts can

be used to optimize the CO₂ desorption from MEA solution and reduce the regeneration energy by 17–24%.²⁴ Following that, in the past decade, a variety of solid acid materials including metal oxides (ZnO, TiO₂, Ag₂O, MoO₃), zeolites (H-Y, SAPO-34), sulfated oxides (SO₄²⁻/ZrO₂/SBA-15), and modified clays (montmorillonite, attapulgite) have been tested to optimize the CO₂ desorption from aqueous monoethanolamine solution at 86–98 °C.^{25–29} Table S1 in the Supporting Information compares the performance of some recent solid acid catalysts for the regeneration of aqueous MEA.^{28–34} Besides the concentration of acid sites, the total surface area and mesoporosity of the used material are also claimed to facilitate the CO₂ desorption reactions.³⁵ Nonetheless, this is an emerging approach, mainly limited to semiprecious metals and laboriously synthesized solid acidic materials, with reaction mechanisms that are somewhat unclear.

In this work, we used abundant and environmentally friendly glucose to synthesize isethionic acid (2-hydroxyethane-1-sulfonic acid)-functionalized carbon spheres and use them to optimize the CO₂ desorption from the MEA solution at 86 °C. The surface functionalization and physicochemical properties of the developed materials were thoroughly analyzed using X-ray photoelectron spectroscopy (XPS), X-ray diffraction (XRD), energy-dispersive X-ray analysis (EDX), Fourier transform infrared (FT-IR) spectroscopy, Raman spectroscopy, thermogravimetric analysis (TGA), scanning electron microscopy (SEM), and pyridine FT-IR spectroscopy. The catalytic performance of the developed materials was experimentally evaluated by calculating the CO₂ desorption rate and quantities of the desorbed CO₂. The regeneration energy consumption was also measured in the presence and absence of these materials to calculate the reduction in the regeneration heat duty due to catalyst addition. Chemical species present in the solution were identified and quantified using ¹³C nuclear magnetic resonance (NMR) analysis to understand the reaction mechanism. Finally, the recyclability of the prepared catalyst was confirmed via cyclic uses.

EXPERIMENTAL SECTION

Materials. D-Glucose (99.5%) was purchased from Chem-Supply in Australia. Isethionic acid sodium salt (98%), hydrochloric acid (HCl, 37%), monoethanolamine (MEA, 99%), and deuterium oxide (99% deuterium atoms) were purchased from Sigma-Aldrich and used without further purification. CO₂ (99.995%) and N₂ (99.999%) were supplied by Rivoira.

Synthesis of Spherical Carbon Catalysts. The carbon catalysts were synthesized according to a one-pot hydrothermal procedure, and a schematic diagram of the preparation procedure is shown in Figure 1a. Typically, 15 g of glucose and 3–15 g of isethionic acid were dissolved in 100 mL of Milli-Q water under magnetic stirring. The obtained mixture was put in a stainless-steel hydrothermal autoclave, sealed, and heated at 180 °C for 12 h, followed by cooling down at room temperature. The obtained black suspension was filtered and washed with a copious amount of Milli-Q water to remove unreacted chemicals or byproducts. The obtained material was then filtered and dried in a vacuum oven at 80 °C overnight. To replace sodium ions with hydrogen ions, post-functionalization of the prepared catalysts was performed using HCl solution. 5 g of each material was mixed with 500 mL of 0.1M HCl solution and continuously stirred at 80 °C for 12 h. The materials were then separated, washed with water, and oven-dried at 80 °C for 8 h. The prepared carbon catalysts were sealed and labeled as CI-X, where X represents the amount of isethionic acid (g) initially dissolved in 100 mL of glucose solution. To study the effect of isethionic acid on the formation of carbon spheres and their physicochemical characteristics, one sample was

synthesized without adding isethionic acid and labeled as CI-0. Due to the formation of carbon spheres in a nanoscale range during the hydrothermal carbonization of pure glucose, CI-0 nanomaterials were separated from the solution and washed by centrifugation (10,000 rpm, 30 min) rather than filtration.

Characterization Methods. Scanning electron microscopy (SEM) was carried out using an FEI Teneo instrument, and all of the samples were coated with 5 nm gold before taking SEM images. X-ray diffraction (XRD) patterns were acquired on a Bruker D8 Advance instrument (Cu K α radiation, 40 mA and 40 kV). Raman spectroscopy was carried out on an inViaTM Qontor confocal Renishaw with a 532 nm laser wavelength. The exterior surface composition of the materials was carefully characterized using X-ray photoelectron spectroscopy (XPS, VG ESCALAB 220i-XL) with Al K α radiation under severe vacuum with 1.0 and 0.05 eV resolution for the broad survey and high-resolution scans, respectively. Fourier transform infrared spectroscopy (FT-IR, Tensor II Bruker) was used in the 400–4000 cm⁻¹ range and 4 cm⁻¹ resolution to analyze the chemical bonds of the prepared materials. The thermal decomposition of the materials was also monitored using thermogravimetric analysis (TGA, NETZSCH TG 209 F1 Libra) using nitrogen as the protective gas (5 °C/min rate). The surface acidity was measured by FT-IR analysis using pyridine as probe molecules. The samples were mixed with KBr to prepare pellets (11 ton, 1 cm²), which were then dehydrated at 150 °C for 2 h before introducing the pyridine vapors. The physisorbed pyridine was removed by heating the IR cell at 150 °C for 1 h under vacuum. Chemical species in solution were identified and quantified by ¹³C NMR analysis performed on samples taken during desorption of each solution, with and without catalysts, at predetermined time intervals, namely, at 5, 10, 15, 25, and 45 min. Spectra were obtained with a Bruker Avance III 400 spectrometer operating at 100.613 MHz by using a procedure already proven in previous work.^{36,37} Details of the experimental settings and methods used to calculate the amounts of each species in the solution are given in the Supporting Information.

CO₂ Absorption and Desorption Experiments. Before studying CO₂ desorption, the 30 wt % MEA solution was enriched with pure CO₂ in a Drechsel gas washing bottle equipped with a glass diffuser (16–40 μm pores). The absorption was performed at the typical absorber temperature, i.e., 40 °C, by placing the Drechsel gas washing bottle in a thermostated bath (Julabo F33-MC bath). The solution was continuously fed with CO₂ until saturation, and the CO₂-rich loading (mol CO₂/mol amine) was computed from the weight increase of the CO₂-saturated solution.³⁸

The CO₂ desorption experiments were performed using the experimental apparatus shown in Figure S1. Briefly, 25 mL of CO₂-saturated amine was charged in a 50 mL conical flask submerged in an oil bath (IKA heating bath HBR 4) and kept constant at 86 °C. A glass condenser was mounted on top of the flask to minimize water vaporization and amine loss. The solution was continuously stirred throughout the regeneration experiment using a magnetic stirrer bar (800 rpm). Pure N₂ (410 mL/min) was introduced in the flask, above the liquid level, to act as a carrier gas and to avoid CO₂ accumulation in the system. The flow rate of N₂ was regulated by means of a digital gas mass flow controller (Aalborg) and a gas meter (Cole Parmer). The CO₂+N₂ gas mixture passed through the glass condenser, followed by a phosphorus pentoxide (P₂O₅) column to remove possible moisture, before being evaluated using a gas chromatograph (Varian CP-4900), equipped with a PoraPLOT U column (Agilent) and a thermal conductivity detector (TCD). For catalytic experiments, 3 wt % of the respective catalyst was added to 25 mL of CO₂-saturated amine at room temperature. The total duration of each experiment was 45 min. To ensure the reliability and reproducibility of CO₂ desorption experiments, two sets of experiments were performed; in the first set, the CO₂ desorption was recorded uninterrupted, while in the second set, liquid samples were taken at predetermined time intervals for NMR analysis to identify and quantify the chemical species present in the liquid solution. The average deviation in the CO₂ desorption rate values was under 1.5%, confirming the reliability and reproducibility of the obtained results.

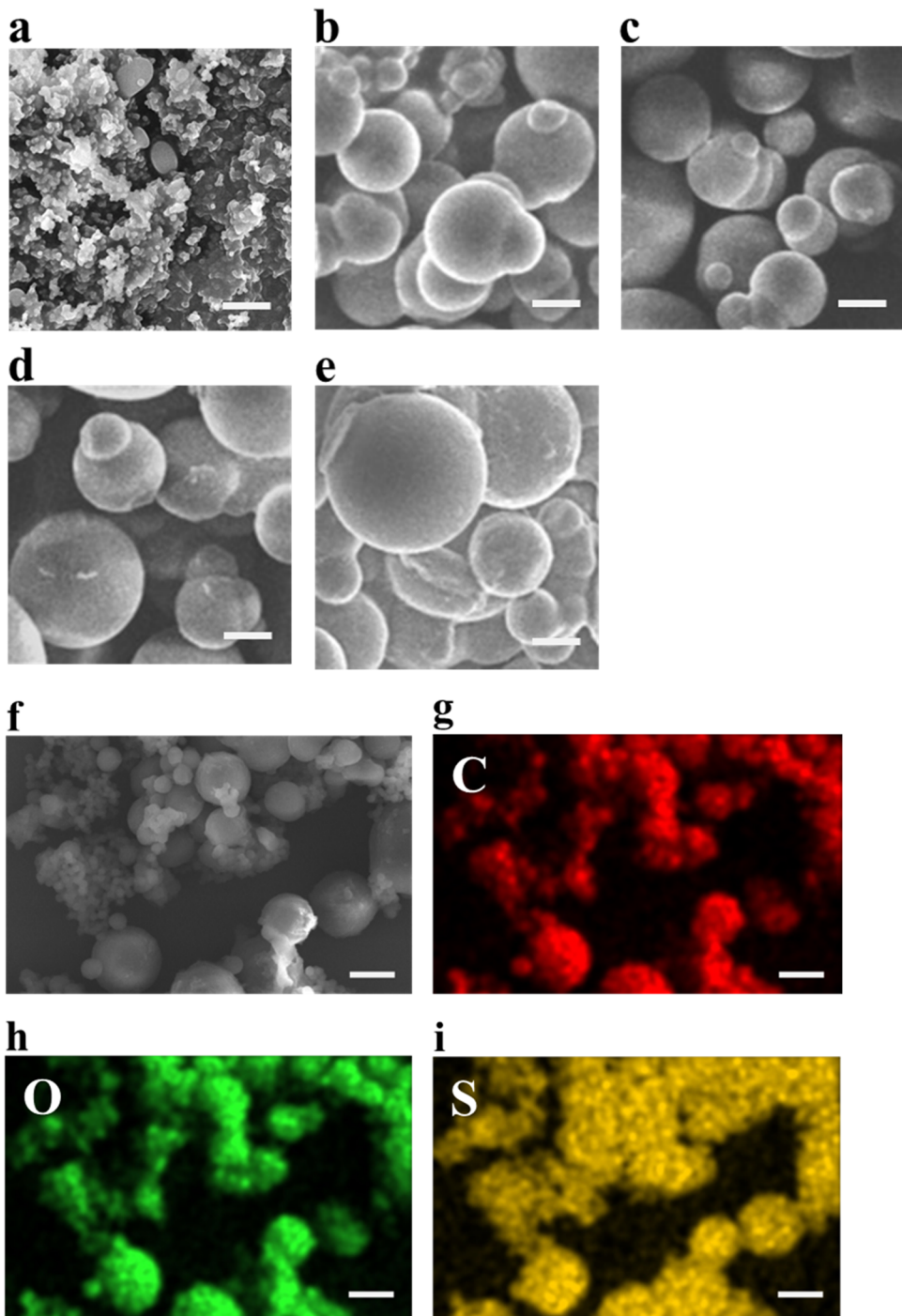


Figure 2. SEM images of (a) CI-0, (b) CI-3, (c) CI-5, (d) CI-10, and (e) CI-15. Scale bars are $2\ \mu\text{m}$. (f–i) EDX mapping of CI-15. Scale bars are 100 nm.

The energy consumption of solvent regeneration experiments was calculated by a power meter (Wattman HPM-100A) with an accuracy of 0.01 kWh. The data calculation methods are provided in the Supporting Information.

RESULTS AND DISCUSSION

Characterization of Catalysts. The thermal stability of the prepared materials was investigated using TGA as shown in Figure 1b. For all materials, initial weight loss of nearly 2 wt % occurring under 100 °C is ascribed to the physically adsorbed water.³⁹ A gradual weight loss was observed for the carbon spheres from 200 to 300 °C due to the disintegration of

sulfonic functional groups.⁴⁰ The weight loss from 300 to 800 °C can be attributed to carbon pyrolysis to form a cross-linking ring structure.⁴⁰ The TGA revealed that the thermal stability of prepared materials is up to 200 °C, which agrees with the published reports.^{39,40} The structure of the prepared materials was explored using Raman scattering spectroscopy as shown in Figure 1c. The band at $1354\ \text{cm}^{-1}$ (D-band) is attributed to the disorderly induced characteristic peak of amorphous carbon, whereas the band at $1590\ \text{cm}^{-1}$ (G-band) is attributed to the stretching vibration of sp^2 carbon,^{39,41} suggesting the amorphous nature of the carbon spheres which is also confirmed by the XRD results (Figure S2). Interestingly, the

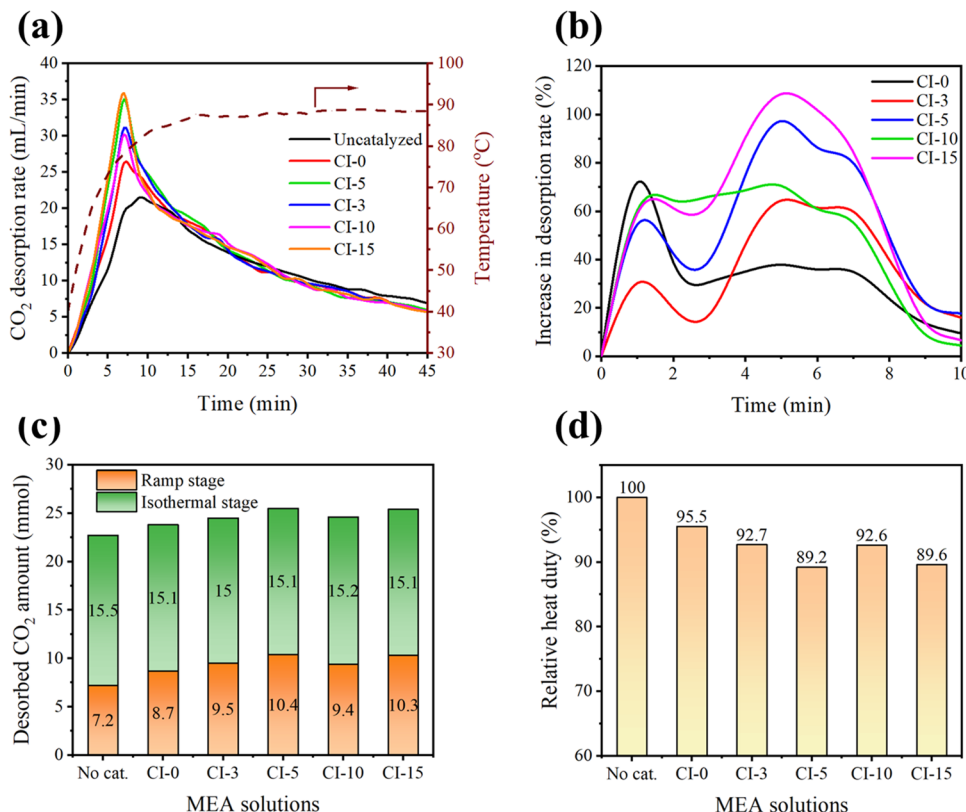


Figure 3. CO₂ desorption performance of MEA solution without and with 3 wt % of each catalyst. (a) CO₂ desorption rate profiles as a function of time and regeneration temperature, (b) increase in the desorption rate from catalytic solutions in comparison with the uncatalyzed solution, (c) quantities of desorbed CO₂ during regeneration experiments, and (d) relative heat duties for MEA solutions.

D-band was almost nonexistent for the nonsulfonated carbon spheres (CI-0) but appeared after the introduction of isethionic acid. It was also revealed that there is a direct relationship between the amount of isethionic acid and D-band intensity, increasing the I_D/I_G ratio from 0.32 in CI-3 to 0.95 in CI-15. This observation indicated that adding isethionic acid during the hydrothermal synthesis of glucose-derived carbon spheres could not only be used as a surface functionalization agent with acidic groups but also change the formation mechanism of carbon spheres, resulting in the creation of new defects within the carbon structure.⁴²

FT-IR spectra of the prepared materials were recorded to obtain information on the structure and functionalization of the carbon spheres (Figure 1d). The broad peak in the region of 3050–3700 cm⁻¹ is attributed to the presence of the hydroxyl group.³⁹ The peak appearing at 2905 cm⁻¹ is ascribed to the C–H stretching vibration in –CH₂ units.⁴¹ The vibration bands appearing at 1026 and 1152 cm⁻¹ are attributed to SO₃⁻ and O=S=O stretching in –SO₃H groups,^{40,42} indicating that the materials possess –SO₃H groups. To further analyze and compare the surface chemical composition of CI-0 and CI-15, before and after sulfonation, XPS was used. The C 1s XPS spectra of CI-0 exhibited a broad peak that can be fitted into three distinct peaks at 284.78, 285.92, and 288.48 eV, indicating the presence of signals from C=C, C–O, and O=C=O bonds, respectively (Figure 1e).⁴⁰ From the O 1s XPS spectra of CI-0 shown in Figure S3, the binding energies at 531.98 and 533.48 eV are assigned to C=O and C–OH bonds.⁴³ The C 1s spectra of CI-15 is deconvoluted into three peaks at 284.68, 286.18, and 288.48 eV associated with the signal from C=C, C–O, and O=C=O

bonds, respectively (Figure S3). The chemical state of sulfur in the CI-15 was characterized by XPS spectra in the S 2p binding energy region, and the recorded peak was deconvoluted into three dominant components at 163.65, 167.58, and 168.88 eV corresponding to the C–S–C bond, S 2p_{3/2} state, and S 2p_{1/2} state of –SO₃H groups (Figure 1f),^{44,45} confirming the successful introduction of –SO₃H groups on the carbon spheres.

The nature of the acidic sites on the surface of carbon spheres was analyzed using pyridine IR spectra as shown in Figure 1g. The peak at 1442 cm⁻¹ is attributed to the presence of Lewis acid sites originating from the functionality of the S=O bonds.⁴⁶ The peak appearing at 1540 cm⁻¹ is ascribed to the Brønsted acid sites due to the formation of pyridinium ions through the interaction of pyridine with the –SO₃H and OH groups.⁴⁷ The peak appearing at ~1492 cm⁻¹ can be attributed to a mixture of Lewis and Brønsted acid sites.

The morphology of the prepared materials was investigated using SEM analysis as shown in Figure 2a–e. According to Figure 2a, the pristine CI-0 carbon without using any isethionic acid had uniformly dispersed spheres with an average diameter of ~180 nm. Although the small size of CI-0 (derived from hydrothermal carbonization of pure glucose) has facilitated the employment of these nanoparticles in a variety of different applications, it can be highlighted as a drawback for the preparation of solid acid catalysts with a nondispersible nature in the liquid phase. On the other hand, all CI-3 to CI-15 samples exhibited very large carbon spheres in the microrange that can be easily filtered out and thus used as solid acid catalysts in the amine regeneration process. The average diameter of the carbon spheres gradually increased by

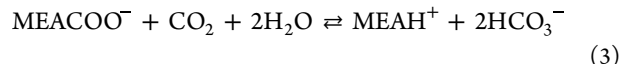
increasing the amount of isethionic acid from $\sim 1.1 \mu\text{m}$ in CI-3 to $\sim 2.8 \mu\text{m}$ in CI-15. Therefore, it can be deduced that isethionic acid molecules can highly accelerate the polymerization of glucose chains at high temperatures, resulting in the formation of large carbon microspheres with some structural deficiencies (as evidenced by Raman spectra). X-ray spectroscopy mapping confirmed the uniform distribution of S and O elements throughout carbon spheres as shown in Figure 2f–i.

CO₂ Desorption Performance. To examine the catalytic activity of the prepared materials, the desorption performance of CO₂-rich MEA solution was first evaluated in the absence of catalysts, and the results were used as a baseline. When studying catalytic regeneration, it is imperative to find out if the presence of solid particles themselves affects the CO₂ desorption. The presence of solid particles in the liquid solution can introduce nucleation sites and enhance the mass transfer rate, thus promoting the CO₂ transfer from the liquid to the gas phase and interfere with the catalytic desorption performance.⁴⁸ To determine the extent of this effect, we first added 3 wt % inert particles to mimic the catalytic desorption scenario. The presence of inactive particles barely changed the CO₂ desorption (Figure S4), implying that any improvement in the desorption rate from catalytic solutions can now be attributed to catalysts' ability to aid CO₂ desorption. For catalytic regeneration experiments, 3 wt % of the respective catalyst was added to 25 mL of CO₂-saturated MEA, and the solution was then regenerated under identical heating conditions. Figure 3a displays CO₂ desorption rate curves for MEA solution in the absence and presence of catalysts. All solutions started to desorb CO₂ from 40 °C onward, and a linear increase in the desorption rate was observed with an increase in the regeneration temperature. The uncatalyzed MEA solution achieved a peak desorption rate of 21.5 mL/min at 9 min, corresponding to 82 °C. All studied catalysts enhanced the CO₂ desorption rate at low temperatures and reduced the time and corresponding temperature for peak CO₂ desorption rate to 7 min, 78 °C. CI-5 and CI-15 were the best-performing catalysts and achieved a similar peak desorption rate of 35.5 mL/min at 78 °C. CI-3 and CI-10 improved the CO₂ desorption rate and achieved the peak desorption rate of 31.1 and 30.2 mL/min, respectively. The CI-0 could also improve the CO₂ desorption rate to 26.3 mL/min. Notably, the developed catalysts optimized the desorption rate at low temperatures (temperature ramp stage) and desorbed up to 108% greater amount of CO₂, compared with the uncatalyzed solution (Figure 3b). CO₂ desorption at low temperatures is crucial to reduce the energy consumption and monetary cost of CO₂ capture as it indicates the possibility that the regenerator column can be operated using waste heat or even hot water. Moreover, faster CO₂ desorption at low temperatures means that the dimensions of the regeneration column can also be reduced.

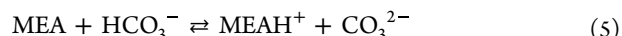
In addition to desorbing greater amounts of CO₂ under identical heating conditions, the catalytic solution shifted the CO₂ desorption to a low-temperature region, i.e., below 86 °C. The uncatalyzed MEA solution could desorb 22.7 mmol of CO₂ throughout the regeneration experiment, with nearly 32% of that quantity being desorbed during the temperature ramp stage (≤ 86 °C corresponding to the first 12 min of regeneration experiments) (Figure 3c). In comparison, the catalytic solutions increased the desorbed quantities of CO₂ by up to 12% and desorbed 37–41% of their respective desorbed quantities during the ramp stage.

The thermal energy required for solvent regeneration is a crucial parameter to assess the energy efficiency of the absorption-based CO₂ capture process. The fact that catalytic solutions released greater amounts of CO₂ in comparison with the uncatalyzed MEA solution under identical heating conditions means that less thermal energy would be required to strip off one mol of CO₂ from the catalytic solutions. The uncatalyzed solution had a heat duty of 257.7 kJ/mol during the 45 min regeneration experiment (Table S2), slightly higher than those reported in the literature.⁴⁹ This is because some energy is lost when electricity is converted to thermal energy, and the reactor was not insulated, meaning that heat loss to the surrounding would have some impact. The heat duty of the uncatalyzed MEA solution was used as a baseline for comparison with the heat duties of the catalytic solutions. The catalytic solution lowered the heat duty by up to 4.5–10.8%, with CI-5 making the highest reduction (Figure 3d).

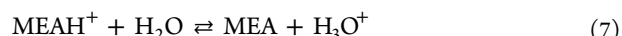
Catalytic Desorption Mechanism. The most widely accepted reaction mechanism for CO₂ absorption in aqueous solutions of primary amine suggests that CO₂ absorption takes place via zwitterion formation. One molecule of MEA reacts with CO₂ to form zwitterion, which then reacts with another MEA molecule to produce carbamate (MEACOO[−]) and protonated amine (MEA^{H+}), as shown by eqs 1 and 2.²¹ At high CO₂ loadings, some of the carbamates can hydrolyze to form MEA and HCO₃[−] (eq 3).



The other main reactions that describe the CO₂ capture by aqueous MEA involve the formation of carbonate and bicarbonate ions⁵⁰



CO₂ desorption is achieved by reversing these reactions. In particular, two main steps are followed: the deprotonation of MEAH⁺ (eq 7) and the carbamate breakdown (eq 8).



However, the proton transfer from protonated amine to water (eq 7) is highly endothermic leading to a lack of free protons available for carbamate breakdown. Therefore, large thermal energy is required for CO₂ desorption. The presence of HCO₃[−] plays a vital role in amine regeneration as it can accept the proton from MEAH⁺ and transfer it to water, thereby dividing a single energy-intensive step of proton transfer into two (eqs 9 and 10). Moreover, carbonic acid can also decompose to release CO₂ (eq 11). Once all HCO₃[−] is consumed, CO₂ desorption mainly depends on carbamate decomposition.



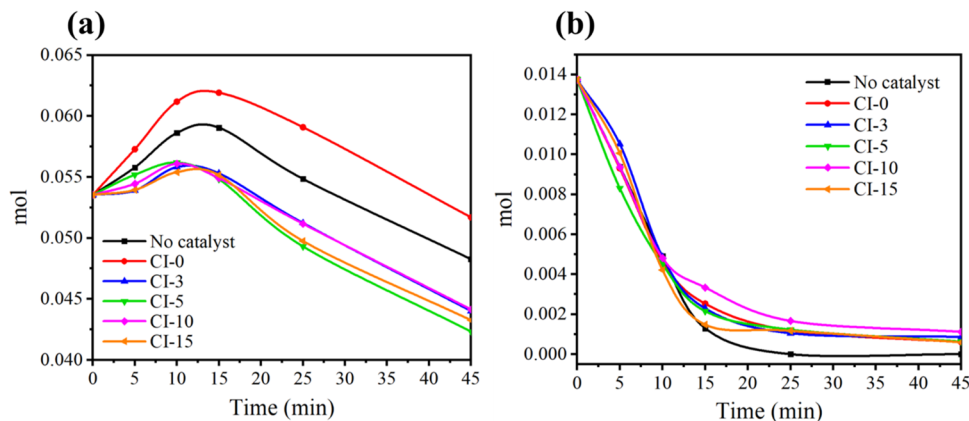
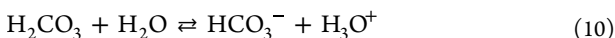


Figure 4. Number of moles of (a) carbamate and (b) bicarbonate/carbonate in MEA solutions as a function of desorption time.



¹³C NMR Speciation Study. To understand the reaction mechanism and catalytic activity of the prepared materials in MEA regeneration, liquid samples of each solution, without and with 3 wt % catalysts, were taken at 5, 10, 15, 25, and 45 min and analyzed by ¹³C NMR, in order to identify and quantify the different species present in solution during the CO₂ desorption process. Detailed speciation over time for each solution is shown in Figure S5 in the Supporting Information.

Figure 4 shows the amounts of carbamate and bicarbonate (more correctly, sum of HCO₃⁻ and CO₃²⁻ ions) as a function of desorption time in both the presence and absence of catalysts, calculated using ¹³C NMR analysis.

For the uncatalyzed MEA solution, it can be observed that in the first 15 min, the amount of carbamate in the solution increases, while the amount of bicarbonate/carbonate rapidly decreases. This is because the bicarbonates react with protonated amines to form carbamate, water, and CO₂, as expressed in (reverse) eq 3. Indeed, after 15 min, the total increase in carbamate (+0.006 mol) is consistent with the decrease of bicarbonate/carbonate (-0.012 mol). Moreover, the amount of MEAH⁺ quickly decreases at the same time (Figure S6). Then, by continuing the desorption, with the bicarbonate/carbonate almost completely consumed, the amount of carbamate begins to decrease significantly.

On the other hand, when glucose catalysts are present in the MEA solution, the initial increase in carbamate is very limited (except for CI-0) and begins to decrease considerably as early as 10 min, while the bicarbonate/carbonate decomposes at nearly a similar rate, clearly indicating the availability of an alternative carbamate breakdown pathway. The acidity of the catalyst speeds up the decomposition of bicarbonate/carbonate, and in fact, between 5 and 10 min, the highest values of desorption rate are recorded.

The NMR data for the CI-0 catalyst conflicts with its CO₂ desorption rate measured from the GC. As an explanation, it is possible that the nonsulfonated carbon spheres are being partially decomposed in the highly basic solution. In fact, the TGA data shows that the CI-0 is relatively less stable among the studied materials. It is quite possible that some other undesired chemical species were released in the solution due to the partial disintegration of glucose-derived carbon spheres in

the CO₂-rich MEA solution. Nonetheless, this observation requires further investigation.

A plausible reaction scheme for glucose catalyst-assisted CO₂ desorption is shown in Figure 5. In the presence of

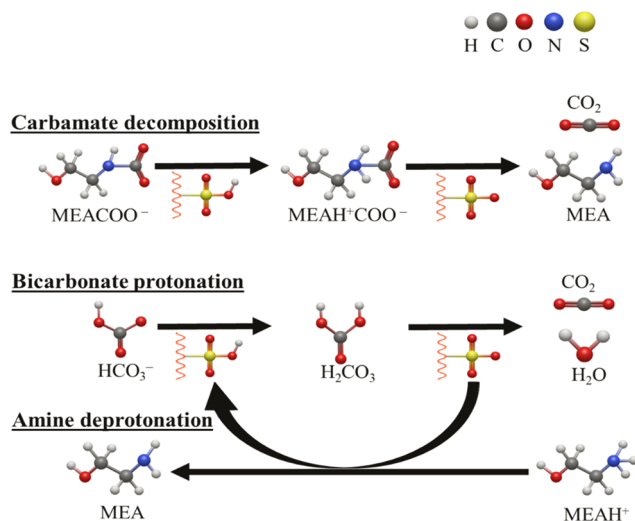
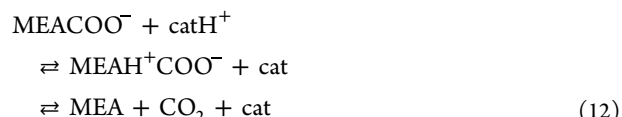


Figure 5. Plausible catalytic mechanism for the functionalized glucose catalyst-aided CO₂ desorption process.

glucose-derived carbon sphere nanocatalysts, additional protons are now available in the system that can facilitate CO₂ release. As the ¹³C NMR results revealed, for catalytic solutions, the amount of bicarbonate decreased without a significant increase in the carbamate concentration, indicating that a new reaction pathway is available in the presence of glucose-based nanocatalysts. The catalysts can provide protons to carbamate to form zwitterion, which can then decompose to release CO₂ (eq 12). Bicarbonates can also obtain protons to form carbonic acid, ultimately decomposing into CO₂ and H₂O (eq 13). In addition to that, the catalyst can accept protons from the protonated amines to accelerate amine regeneration, as shown in eq 14.



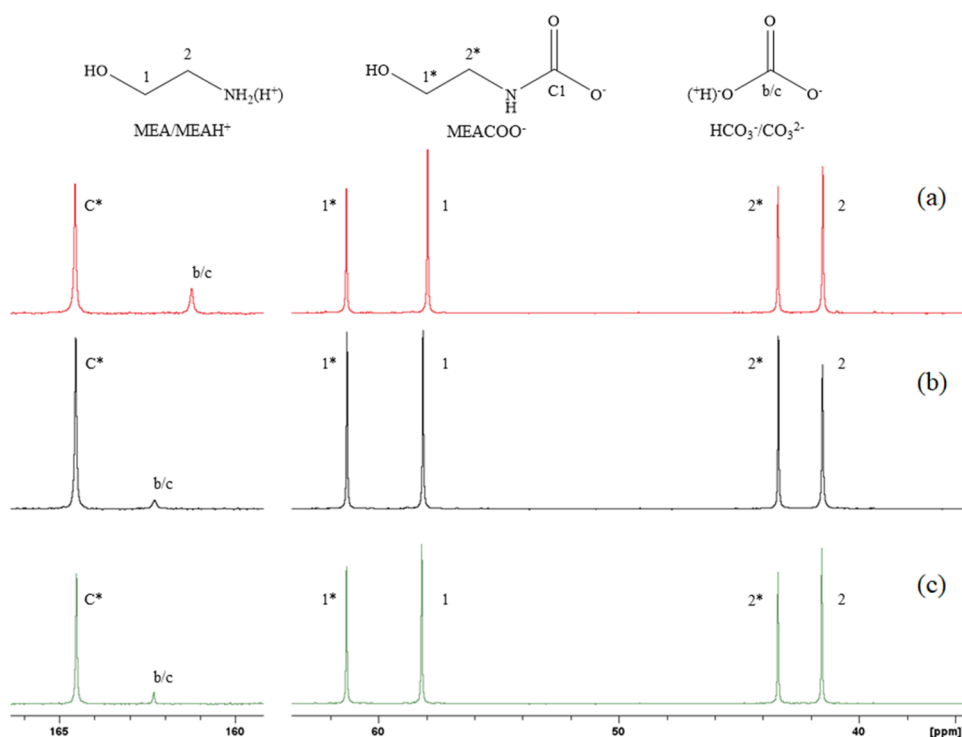


Figure 6. (a) ^{13}C NMR spectra of CO_2 -loaded MEA; ^{13}C NMR spectra after 10 min of desorption at $T = 86\text{ }^\circ\text{C}$ for (b) blank and (c) CI-15. The height of the peaks at 160–165 ppm is not in scale.



Confirming the hypothesis, Figure 6 shows the ^{13}C NMR spectra of the CO_2 -saturated MEA solution, after 10 min of desorption with or without the catalyst (CI-15 is shown here). As observed, for the same desorption time, the amount of carbamate is lower in the presence of a catalyst.

Catalyst Stability and Reusability. For an industrial application, it is imperative for the catalyst to remain stable without a significant loss in its activity. To confirm the stability of the prepared catalysts, CI-15 was used in five cyclic CO_2 desorption tests. For this, 3 wt % CI-15 was added to 25 mL of MEA solution, and the regeneration was studied under the operating conditions described previously. At the end of the regeneration experiment, the catalyst was filtered, repeatedly washed with distilled water, dried, and used for the next CO_2 desorption experiment. The average catalyst mass recovery was around 93%, and a supplementary amount was added to the recovered catalyst before using it in the next CO_2 desorption experiment. At the end of five cycles, the CO_2 desorption rate and desorbed quantity of CO_2 were compared, and a slight reduction in the catalyst performance was observed that could be due to particle agglomeration and deactivation of some active sites. Overall, the catalyst remained active during repeated cycles (Figure 7) and therefore may be used in a continuous CO_2 capture process.

CONCLUSIONS

In summary, a series of isethionic acid-functionalized glucose-derived carbon nanocatalysts were prepared and used to optimize the CO_2 desorption from MEA solution at $86\text{ }^\circ\text{C}$, ultimately to develop an energy-efficient CO_2 capture process. The synthesized catalysts accelerated the carbamate breakdown and reduced the temperature for peak CO_2 desorption. While consuming the same amount of thermal energy, the

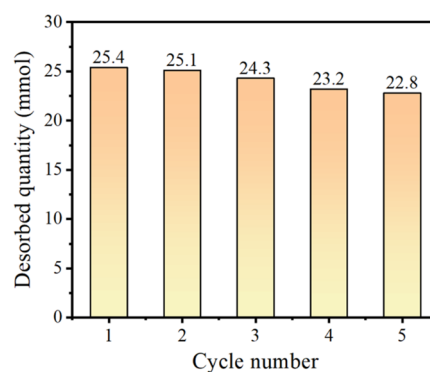


Figure 7. Quantity of desorbed CO_2 from CI-15 catalyst recycling experiments.

developed catalysts increased the CO_2 desorption rate and desorbed quantity of CO_2 by 108 and 12%, respectively, and consequently lowered the relative heat duty by 10.8%, compared to the uncatalyzed MEA solution. To elucidate the catalytic activity and reaction mechanism, liquid samples were taken during the regeneration of MEA without and with each catalyst at specific time intervals and were analyzed using ^{13}C NMR. It was revealed that the catalysts provide protons to the carbamate and bicarbonate to accelerate the CO_2 release at low temperatures. The ^{13}C NMR speciation data for MEA solution without and with developed catalysts was compared and used to propose a reaction mechanism for carbon sphere nanocatalyst-aided CO_2 desorption. Finally, the catalyst stability and reusability were tested via cyclic use, which confirmed their potential to be used in a stripper column for energy-efficient CO_2 capture processes.

ASSOCIATED CONTENT

Supporting Information

The Supporting Information is available free of charge at <https://pubs.acs.org/doi/10.1021/acssuschemeng.3c02069>.

Additional experimental details, analytical results, and calculation methods ([PDF](#))

AUTHOR INFORMATION

Corresponding Authors

Jorge Gascon – KAUST Catalysis Center (KCC), King Abdullah University of Science and Technology (KAUST), Thuwal 23955, Saudi Arabia; orcid.org/0000-0001-7558-7123; Email: Jorge.gascon@kaust.edu.sa

Kathryn A. Mumford – Department of Chemical Engineering, The University of Melbourne, Victoria 3010, Australia; orcid.org/0000-0002-7056-5600; Email: mumfordk@unimelb.edu.au

Authors

Umair H. Bhatti – KAUST Catalysis Center (KCC), King Abdullah University of Science and Technology (KAUST), Thuwal 23955, Saudi Arabia; orcid.org/0000-0003-3565-7582

Masood S. Alivand – Department of Chemical Engineering, The University of Melbourne, Victoria 3010, Australia; Department of Chemical Engineering, Monash University, Victoria 3800, Australia

Francesco Barzagli – National Research Council (CNR), ICCOM Institute, 50019 Sesto Fiorentino, Florence, Italy; orcid.org/0000-0002-5077-0420

Meher Geetika Sanku – National Research Council (CNR), ICCOM Institute, 50019 Sesto Fiorentino, Florence, Italy; orcid.org/0000-0002-8829-8918

Complete contact information is available at:

<https://pubs.acs.org/10.1021/acssuschemeng.3c02069>

Notes

The authors declare no competing financial interest.

ACKNOWLEDGMENTS

This research was conducted in part at the Advanced Separation Technologies, Bio21 Advanced Microscopy Facility, and Materials Characterization and Fabrication Platform (MCFP) at the University of Melbourne. The authors also acknowledge the ICCOM Institute of the Italian National Research Council for the NMR analysis and the financial support through the project SPICCO2 (project code DCM.AD004.109), and the financial support from the Hans Werthén fund managed by the Royal Swedish Academy of Engineering Sciences (IVA, Stockholm).

REFERENCES

- (1) Global Energy Review. CO₂ Emissions in 2021 – Analysis - IEA. 2022 <https://www.iea.org/reports/global-energy-review-co2-emissions-in-2021-2> (accessed Oct 16, 2022).
- (2) Lai, Q.; Toan, S.; Assiri, M. A.; Cheng, H.; Russell, A. G.; Adidharma, H.; Radosz, M.; Fan, M. Catalyst-TiO(OH)₂ Could Drastically Reduce the Energy Consumption of CO₂ Capture. *Nat. Commun.* **2018**, *9*, No. 2672.
- (3) Feron, P. H. M.; Cousins, A.; Jiang, K.; Zhai, R.; Garcia, M. An Update of the Benchmark Post-Combustion CO₂-Capture Technology. *Fuel* **2020**, *273*, No. 117776.
- (4) Asif, M.; Suleman, M.; Haq, I.; Jamal, S. A. Post-Combustion CO₂ Capture with Chemical Absorption and Hybrid System: Current Status and Challenges. *Greenhouse Gases: Sci. Technol.* **2018**, *8*, 998–1031.
- (5) Mumford, K. A.; Wu, Y.; Smith, K. H.; Stevens, G. W. Review of Solvent Based Carbon-Dioxide Capture Technologies. In *Front Chem Sci Eng*; Higher Education Press, June 24, 2015; pp 125–141 DOI: [10.1007/s11705-015-1514-6](https://doi.org/10.1007/s11705-015-1514-6).
- (6) Bhatti, U. H.; Sultan, H.; Min, G. H.; Nam, S. C.; Baek, I. H. Ion-Exchanged Montmorillonite as Simple and Effective Catalysts for Efficient CO₂ Capture. *Chem. Eng. J.* **2020**, *413*, No. 127476.
- (7) Xie, H.; Wu, Y.; Liu, T.; Wang, F.; Chen, B.; Liang, B. Low-Energy-Consumption Electrochemical CO₂ Capture Driven by Biomimetic Phenazine Derivatives Redox Medium. *Appl. Energy* **2020**, *259*, No. 114119.
- (8) Shi, H.; Zheng, L.; Huang, M.; Zuo, Y.; Li, M.; Jiang, L.; Idem, R.; Tontiwachwuthikul, P. CO₂ Desorption Tests of Blended Monoethanolamine–Diethanolamine Solutions to Discover Novel Energy Efficient Solvents. *Asia-Pac. J. Chem. Eng.* **2018**, *13*, No. e2186.
- (9) Wang, R.; Liu, S.; Li, Q.; Zhang, S.; Wang, L.; An, S. CO₂ Capture Performance and Mechanism of Blended Amine Solvents Regulated by N-Methylcyclohexylamine. *Energy* **2021**, *215*, No. 119209.
- (10) Chen, G.; Chen, G.; Peruzzini, M.; Zhang, R.; Barzagli, F. Understanding the Potential Benefits of Blended Ternary Amine Systems for CO₂ Capture Processes through ¹³C NMR Speciation Study and Energy Cost Analysis. *Sep. Purif. Technol.* **2022**, *291*, No. 120939.
- (11) Wang, L.; Liu, S.; Wang, R.; Li, Q.; Zhang, S. Regulating Phase Separation Behavior of a DEEA-TETA Biphasic Solvent Using Sulfolane for Energy-Saving CO₂ Capture. *Environ. Sci. Technol.* **2019**, *53*, 12873–12881.
- (12) Jiang, C.; Chen, H.; Wang, J.; Shen, Y.; Ye, J.; Zhang, S.; Wang, L.; Chen, J. Phase Splitting Agent Regulated Biphasic Solvent for Efficient CO₂ Capture with a Low Heat Duty. *Environ. Sci. Technol.* **2020**, *54*, 7601–7610.
- (13) Barzagli, F.; Mani, F.; Peruzzini, M. Novel Water-Free Biphasic Absorbents for Efficient CO₂ Capture. *Int. J. Greenhouse Gas Control* **2017**, *60*, 100–109.
- (14) Saeed, U.; Khan, A. L.; Gilani, M. A.; Bilad, M. R.; Khan, A. U. Supported Deep Eutectic Liquid Membranes with Highly Selective Interaction Sites for Efficient CO₂ Separation. *J. Mol. Liq.* **2021**, *342*, No. 117509.
- (15) Trivedi, T. J.; Lee, J. H.; Lee, H. J.; Jeong, Y. K.; Choi, J. W. Deep Eutectic Solvents as Attractive Media for CO₂ Capture. *Green Chem.* **2016**, *18*, 2834–2842.
- (16) Hwang, J.; Kim, J.; Lee, H. W.; Na, J.; Ahn, B. S.; Lee, S. D.; Kim, H. S.; Lee, H.; Lee, U. An Experimental Based Optimization of a Novel Water Lean Amine Solvent for Post Combustion CO₂ Capture Process. *Appl. Energy* **2019**, *248*, 174–184.
- (17) Guo, H.; Li, C.; Shi, X.; Li, H.; Shen, S. Nonaqueous Amine-Based Absorbents for Energy Efficient CO₂ Capture. *Appl. Energy* **2019**, *239*, 725–734.
- (18) Wanderley, R. R.; Pinto, D. D. D.; Knuutila, H. K. From Hybrid Solvents to Water-Lean Solvents – A Critical and Historical Review. *Sep. Purif. Technol.* **2021**, *260*, No. 118193.
- (19) Xu, Y.; Fang, M.; Yang, Q.; Xia, Z.; Yu, H.; Wang, T.; Chen, K.; Puxty, G. Diamine Based Water-Lean CO₂ Solvent with Extra High Cyclic Capacity and Low Viscosity. *Greenhouse Gases: Sci. Technol.* **2021**, *11*, 828–836.
- (20) Vega, F.; Baena-Moreno, F. M.; Gallego Fernández, L. M.; Portillo, E.; Navarrete, B.; Zhang, Z. Current Status of CO₂ Chemical Absorption Research Applied to CCS: Towards Full Deployment at Industrial Scale. *Appl. Energy* **2020**, *260*, No. 114313.
- (21) Alivand, M. S.; Mazaheri, O.; Wu, Y.; Stevens, G. W.; Scholes, C. A.; Mumford, K. A. Catalytic Solvent Regeneration for Energy-Efficient CO₂ Capture. *ACS Sustainable Chem. Eng.* **2020**, *8*, 18755–18788.

- (22) Bhatti, U. H.; Ienco, A.; Peruzzini, M.; Barzagli, F. Unraveling the Role of Metal Oxide Catalysts in the CO₂Desorption Process from Nonaqueous Sorbents: An Experimental Study Carried out with ¹³C NMR. *ACS Sustainable Chem. Eng.* **2021**, *9*, 15419–15426.
- (23) Alivand, M. S.; Mazaheri, O.; Wu, Y.; Zavabeti, A.; Christofferson, A. J.; Meftahi, N.; Russo, S. P.; Stevens, G. W.; Scholes, C. A.; Mumford, K. A. Engineered Assembly of Water-Dispersible Nanocatalysts Enables Low-Cost and Green CO₂ Capture. *Nat. Commun.* **2022**, *13*, No. 1249.
- (24) Idem, R.; Shi, H.; Gelowitz, D.; Tontiwachwuthikul, P. Catalytic Method and Apparatus for Separating a Gaseous Component from an Incoming Gas Stream. Patent WO2011120138A1, 2011.
- (25) Bhatti, U. H.; Shah, A. K.; Kim, J. N.; You, J. K.; Choi, S. H.; Lim, D. H.; Nam, S.; Park, Y. H.; Baek, I. H. Effects of Transition Metal Oxide Catalysts on MEA Solvent Regeneration for the Post-Combustion Carbon Capture Process. *ACS Sustainable Chem. Eng.* **2017**, *5*, 5862–5868.
- (26) Bhatti, U. H.; Sivanesan, D.; Lim, D. H.; Nam, S. C.; Park, S.; Baek, I. H. Metal Oxide Catalyst-Aided Solvent Regeneration: A Promising Method to Economize Post-Combustion CO₂ Capture Process. *J. Taiwan Inst. Chem. Eng.* **2018**, *93*, 150–157.
- (27) Zhang, X.; Zhang, X.; Liu, H.; Li, W.; Xiao, M.; Gao, H.; Liang, Z. Reduction of Energy Requirement of CO₂ Desorption from a Rich CO₂-Loaded MEA Solution by Using Solid Acid Catalysts. *Appl. Energy* **2017**, *202*, 673–684.
- (28) Bhatti, U. H.; KAZMI, W. W.; Muhammad, H.; Min, G. H.; Nam, S. C.; Baek, I. H. Practical and Inexpensive Acid-Activated Montmorillonite Catalysts for Energy-Efficient CO₂ Capture. *Green Chem.* **2020**, *22*, 6328–6333.
- (29) Tan, Z.; Zhang, S.; Yue, X.; Zhao, F.; Xi, F.; Yan, D.; Ling, H.; Zhang, R.; Tang, F.; You, K.; Luo, H.; Zhang, X. Attapulgite as a Cost-Effective Catalyst for Low-Energy Consumption Amine-Based CO₂ Capture. *Sep. Purif. Technol.* **2022**, *298*, No. 121577.
- (30) Bhatti, U. H.; Sivanesan, D.; Lim, D. H.; Nam, S. C.; Park, S.; Baek, I. H. Metal Oxide Catalyst-Aided Solvent Regeneration: A Promising Method to Economize Post-Combustion CO₂ Capture Process. *J. Taiwan Inst. Chem. Eng.* **2018**, *93*, 150–157.
- (31) Wang, T.; Yu, W.; Liu, F.; Fang, M.; Farooq, M.; Luo, Z. Enhanced CO₂ Absorption and Desorption by Monoethanolamine (MEA)-Based Nanoparticle Suspensions. *Ind. Eng. Chem. Res.* **2016**, *55*, 7830–7838.
- (32) Xing, L.; Wei, K.; Li, Q.; Wang, R.; Zhang, S.; Wang, L. One-Step Synthesized SO₄²⁻/ZrO₂-HZSM-5 Solid Acid Catalyst for Carbamate Decomposition in CO₂ Capture. *Environ. Sci. Technol.* **2020**, *54*, 13944–13952.
- (33) Xing, L.; Wei, K.; Li, Y.; Fang, Z.; Li, Q.; Qi, T.; An, S.; Zhang, S.; Wang, L. TiO₂Coating Strategy for Robust Catalysis of the Metal-Organic Framework toward Energy-Efficient CO₂Capture. *Environ. Sci. Technol.* **2021**, *55*, 11216–11224.
- (34) Alivand, M. S.; Mazaheri, O.; Wu, Y.; Zavabeti, A.; Stevens, G. W.; Scholes, C. A.; Mumford, K. A. Water-Dispersible Nanocatalysts with Engineered Structures: The New Generation of Nanomaterials for Energy-Efficient CO₂Capture. *ACS Appl. Mater. Interfaces* **2021**, *13*, 57294–57305.
- (35) Bhatti, U. H.; Shah, A. K.; Hussain, A.; Khan, H. A.; Park, C. Y.; Nam, S. C.; Baek, I. H. Catalytic Activity of Facilely Synthesized Mesoporous HZSM-5 Catalysts for Optimizing the CO₂ Desorption Rate from CO₂-Rich Amine Solutions. *Chem. Eng. J.* **2020**, *389*, No. 123439.
- (36) Barzagli, F.; Lai, S.; Mani, F. CO₂ Capture by Liquid Solvents and Their Regeneration by Thermal Decomposition of the Solid Carbonated Derivatives. *Chem. Eng. Technol.* **2013**, *36*, 1847–1852.
- (37) Barzagli, F.; Giorgi, C.; Mani, F.; Peruzzini, M. CO₂ Capture by Aqueous Na₂CO₃ Integrated with High-Quality CaCO₃ Formation and Pure CO₂ Release at Room Conditions. *J. CO₂ Util.* **2017**, *22*, 346–354.
- (38) Zhicheng, X.; Wang, S.; Zhao, B.; Chen, C. Study on Potential Biphasic Solvents: Absorption Capacity, CO₂ Loading and Reaction Rate. *Energy Procedia* **2013**, *37*, 494–498.
- (39) Chen, X.; Zhang, Z.; Yuan, B.; Yu, F.; Xie, C.; Yu, S. Lignin-Based Sulfonated Carbon as an Efficient Biomass Catalyst for Clean Benzylation of Benzene Ring Compounds. *J. Ind. Eng. Chem.* **2022**, *111*, 369–379.
- (40) Song, H.; Xing, C.; Li, B.; Shen, W. Spherical Carbon with SO₃H Groups as an Efficient Solid Acid Catalyst for 2,4,5-Triphenyl-Imidazole Synthesis. *ChemistrySelect* **2016**, *1*, 301–308.
- (41) Ravi, K.; Biradar, A. V. Highly Active and Scalable SO₃H Functionalized Carbon Catalyst Synthesized from Bagasse for Transformation of Bio-Based Platform Chemicals into Fuel Precursors and Its in-Depth Characterization Studies. *Fuel* **2022**, *321*, No. 124008.
- (42) Sun, Y.; Zhang, Q.; Zhang, P.; Song, D.; Guo, Y. Nitrogen-Doped Carbon-Based Acidic Ionic Liquid Hollow Nanospheres for Efficient and Selective Conversion of Fructose to 5-Ethoxymethyl-furfural and Ethyl Levulinate. *ACS Sustainable Chem. Eng.* **2018**, *6*, 6771–6782.
- (43) Konwar, L. J.; Mäki-Arvela, P.; Kumar, N.; Mikkola, J. P.; Sarma, A. K.; Deka, D. Selective Esterification of Fatty Acids with Glycerol to Monoglycerides over –SO₃H Functionalized Carbon Catalysts. *React. Kinet., Mech. Catal.* **2016**, *119*, 121–138.
- (44) Wang, Y.; Wang, D.; Tan, M.; Jiang, B.; Zheng, J.; Tsubaki, N.; Wu, M. Monodispersed Hollow SO₃H-Functionalized Carbon/Silica as Efficient Solid Acid Catalyst for Esterification of Oleic Acid. *ACS Appl. Mater. Interfaces* **2015**, *7*, 26767–26775.
- (45) Malaika, A.; Kozłowski, M. Glycerol Conversion towards Valuable Fuel Blending Compounds with the Assistance of SO₃H-Functionalized Carbon Xerogels and Spheres. *Fuel Process. Technol.* **2019**, *184*, 19–26.
- (46) Upare, P. P.; Yoon, J. W.; Kim, M. Y.; Kang, H. Y.; Hwang, D. W.; Hwang, Y. K.; Kung, H. H.; Chang, J. S. Chemical Conversion of Biomass-Derived Hexose Sugars to Levulinic Acid over Sulfonic Acid-Functionalized Graphene Oxide Catalysts. *Green Chem.* **2013**, *15*, 2935–2943.
- (47) Ghosh, A.; Singha, A.; Auroux, A.; Das, A.; Sen, D.; Chowdhury, B. A Green Approach for the Preparation of a Surfactant Embedded Sulfonated Carbon Catalyst towards Glycerol Acetalization Reactions. *Catal. Sci. Technol.* **2020**, *10*, 4827–4844.
- (48) Bhatti, U. H.; Nam, S.; Park, S.; Baek, I. H. Performance and Mechanism of Metal Oxide Catalyst-Aided Amine Solvent Regeneration. *ACS Sustainable Chem. Eng.* **2018**, *6*, 12079–12087.
- (49) Kim, H.; Hwang, S. J.; Lee, K. S. Novel Shortcut Estimation Method for Regeneration Energy of Amine Solvents in an Absorption-Based Carbon Capture Process. *Environ. Sci. Technol.* **2015**, *49*, 1478–1485.
- (50) Barzagli, F.; Mani, F. Direct CO₂ Air Capture with Aqueous 2-(Ethylamino)Ethanol and 2-(2-Aminoethoxy)Ethanol: ¹³C NMR Speciation of the Absorbed Solutions and Study of the Sorbent Regeneration Improved by a Transition Metal Oxide Catalyst. *Inorg. Chim. Acta* **2021**, *518*, No. 120256.